SHORT COMMUNICATION

Journal of Semiconductors
(2021) 42, 070501
doi: 10.1088/1674-4926/42/7/070501

Post-sulphuration enhances the performance of a lactone polymer donor

Yufan Jiang[1, 2], Ke Jin[2], Xiujuan Chen[2], Zuo Xiao[2, †], Xiaotao Zhang[1, †], and Liming Ding[2, †]

[1]Department of Chemistry, Tianjin University, Tianjin 300072, China

[2]Center for Excellence in Nanoscience (CAS), Key Laboratory of Nanosystem and Hierarchical Fabrication (CAS), National Center for Nanoscience and Technology, Beijing 100190, China

Citation: Y F Jiang, K Jin, X J Chen, Z Xiao, X T Zhang, and L M Ding, Post-sulphuration enhances the performance of a lactone polymer donor[J]. *J. Semicond.*, 2021, 42(7), 070501. http://doi.org/10.1088/1674-4926/42/7/070501

SUPPORTING INFORMATION

1. General characterization

^{1}H and ^{13}C NMR spectra were measured on a Bruker Avance-400 spectrometer. Absorption spectra were recorded on a Shimadzu UV-1800 spectrophotometer. FT-IR spectra were recorded on a Spotlight 200i spectrophotometer. Cyclic voltammetry was done by using a Shanghai Chenhua CHI620D voltammetric analyzer under argon in an anhydrous acetonitrile solution of tetra-n-butylammonium hexafluorophosphate (0.1 M). A glassy-carbon electrode was used as the working electrode, a platinum-wire was used as the counter electrode, and a Ag/Ag$^+$ electrode was used as the reference electrode. L1-S was coated onto glassy-carbon electrode and all potentials were corrected against Fc/Fc$^+$. AFM was performed on a multimode microscope (Veeco) by using tapping mode.

2. Synthesis

All reagents were purchased from J&K Co., Aladdin Co., Innochem Co., Derthon Co. and other commercial suppliers. L1 and M1 was synthesized according to literature[1]. All reac-

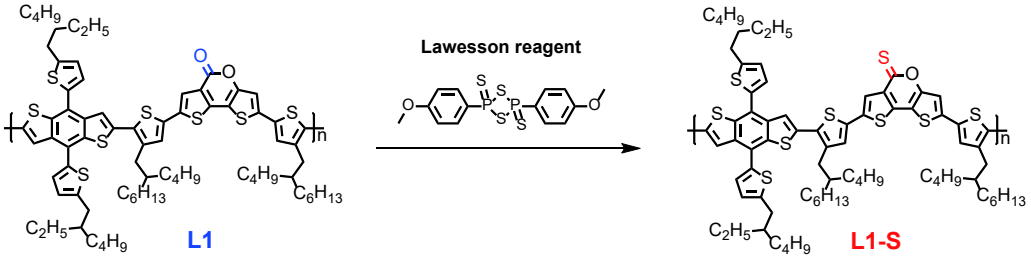

Scheme 1. The post-sulphuration route to L1-S.

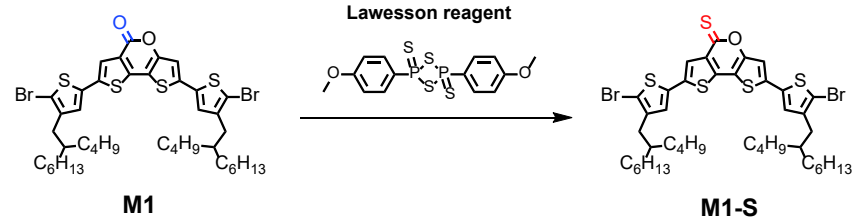

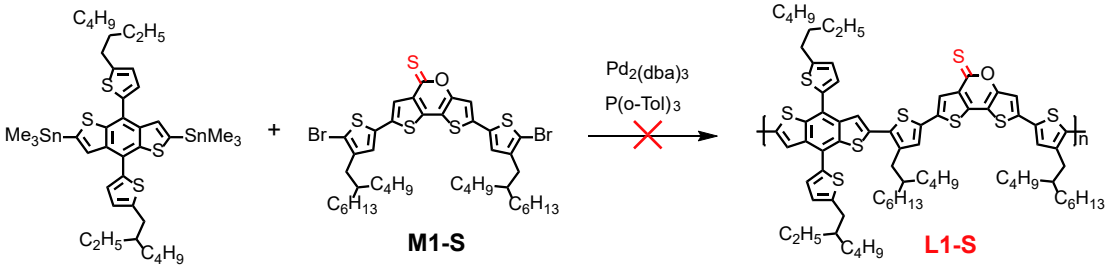

Scheme 2. The failed pre-sulphuration route to L1-S.

Correspondence to: Z Xiao, xiaoz@nanoctr.cn; X T Zhang, zhangxt@tju.edu.cn; L M Ding, ding@nanoctr.cn

Received 24 MAY 2021.

tions dealing with air- or moisture-sensitive compounds were carried out by using standard Schlenk techniques.

L1-S. To a solution of L1 (200 mg, M_n 42.5 kDa, PDI 2.03) in chlorobenzene (15 mL) was added Lawesson reagent (94.4 mg, 0.233 mmol) under argon. The mixture was heated at 120 °C overnight. The color of the solution gradually changed from light-red to dark-red. After cooling to room temperature, the solution passed through a short silica gel column with $CHCl_3$ as the eluent. The solution was concentrated and added into methanol dropwise. The precipitate was collected and dried under vacuum overnight to give L1-S as a brown solid (195 mg, 96%). The M_n for L1-S is 42.8 kDa, with a PDI of 2.05. ^{1}H NMR (ODCB-d4, 403 K, 400 MHz, δ/ppm): 7.77–6.80 (br, aromatic protons), 2.81 (br, aliphatic protons), 1.78–0.76 (br, aliphatic protons).

M1-S. To a solution of M1 (50 mg, 0.058 mmol) in toluene (5 mL) was added Lawesson reagent (35 mg, 0.087 mmol) under argon. The mixture was heated at 110 °C for 3 h. After removal of the solvent, the crude product was purified via column chromatography (silica gel) by using CH_2Cl_2:petroleum ether (1.5 : 1) as eluent. Further precipitation in methanol gave M1-S as an orange solid (26 mg, 51%). ^{1}H NMR ($CDCl_3$, 400 MHz, δ/ppm): 7.64 (s, 1H), 7.04 (s, 1H), 6.94 (s, 1H), 6.88 (s, 1H), 2.48 (dd, J = 6.8, 5.3 Hz, 4H), 1.67 (br, 2H), 1.29–1.28 (m, 32H), 0.92-0.87 (m, 12H). ^{13}C NMR ($CDCl_3$, 100 MHz, δ/ppm): 189.89, 155.58, 143.06, 142.70, 138.01, 137.63, 135.67, 135.37, 134.55, 134.28, 126.89, 126.77, 124.36, 114.88, 112.51, 111.86, 111.08, 38.52, 34.16, 32.98, 31.88, 29.67, 28.71, 26.47, 23.04, 22.68, 14.13.

3. NMR

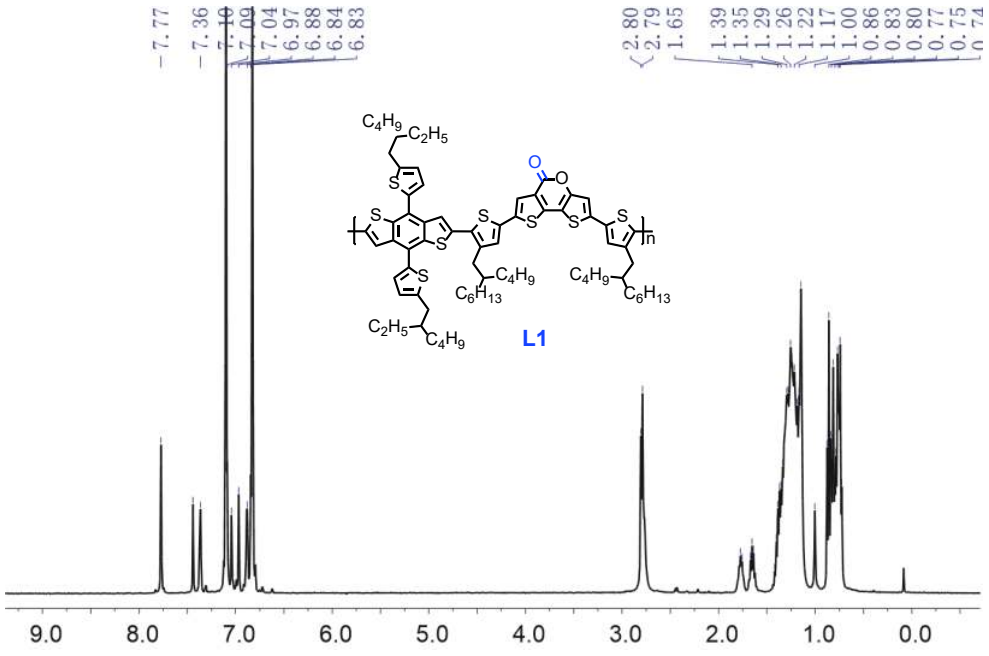

Fig. S1. ^{1}H NMR spectrum of the starting material L1 (ODCB-d4, 403 K).

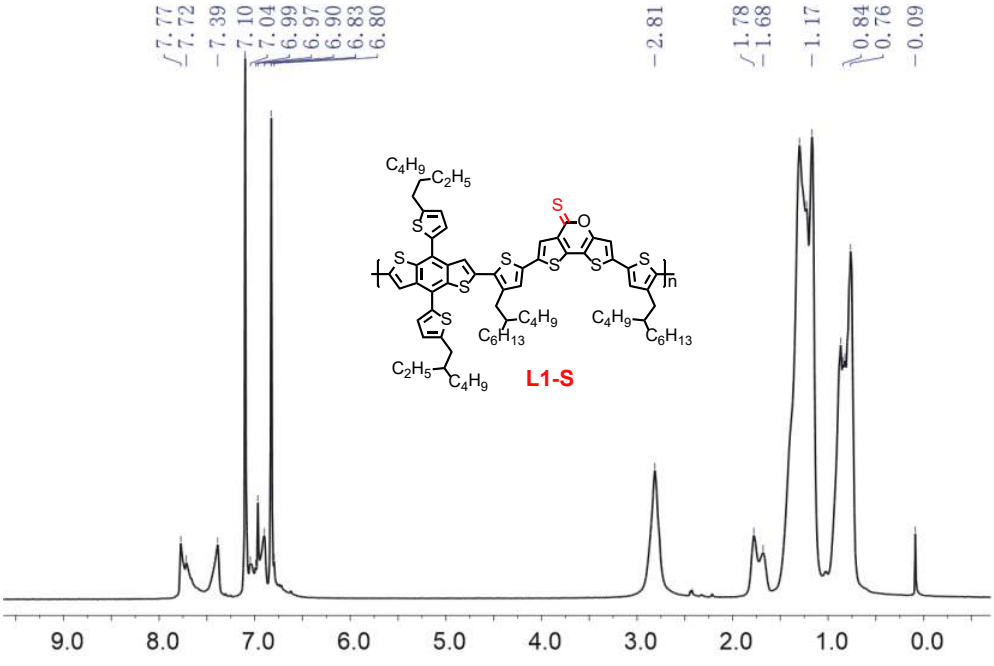

Fig. S2. ^{1}H NMR spectrum of L1-S (ODCB-d4, 403 K).

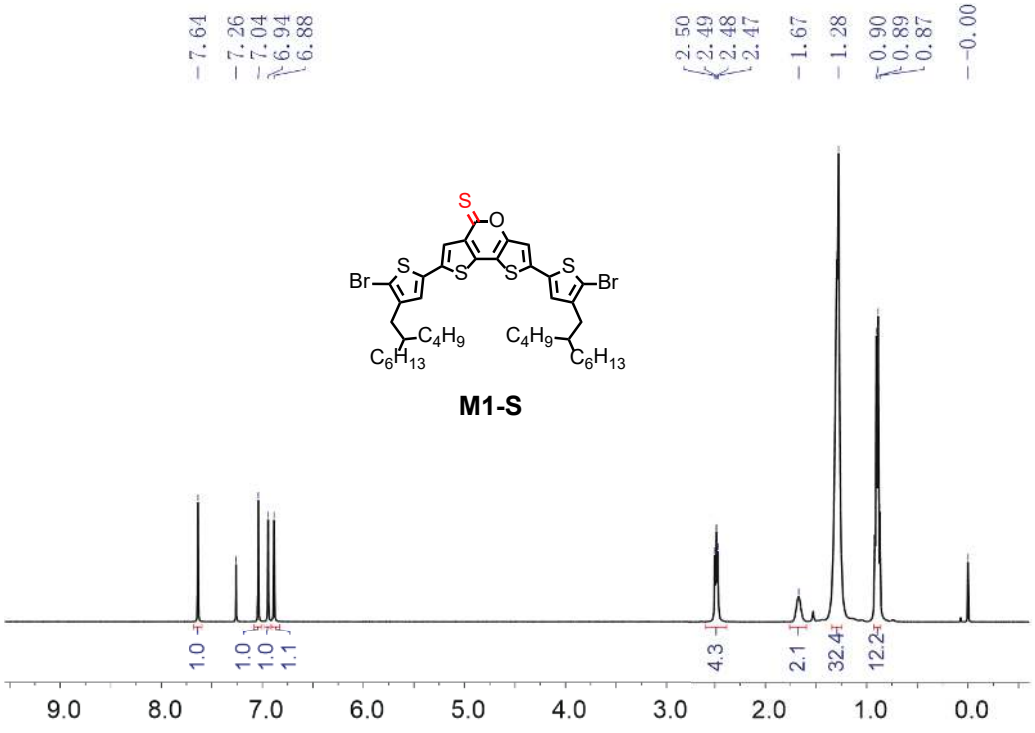

Fig. S3. ^{1}H NMR spectrum of M1-S.

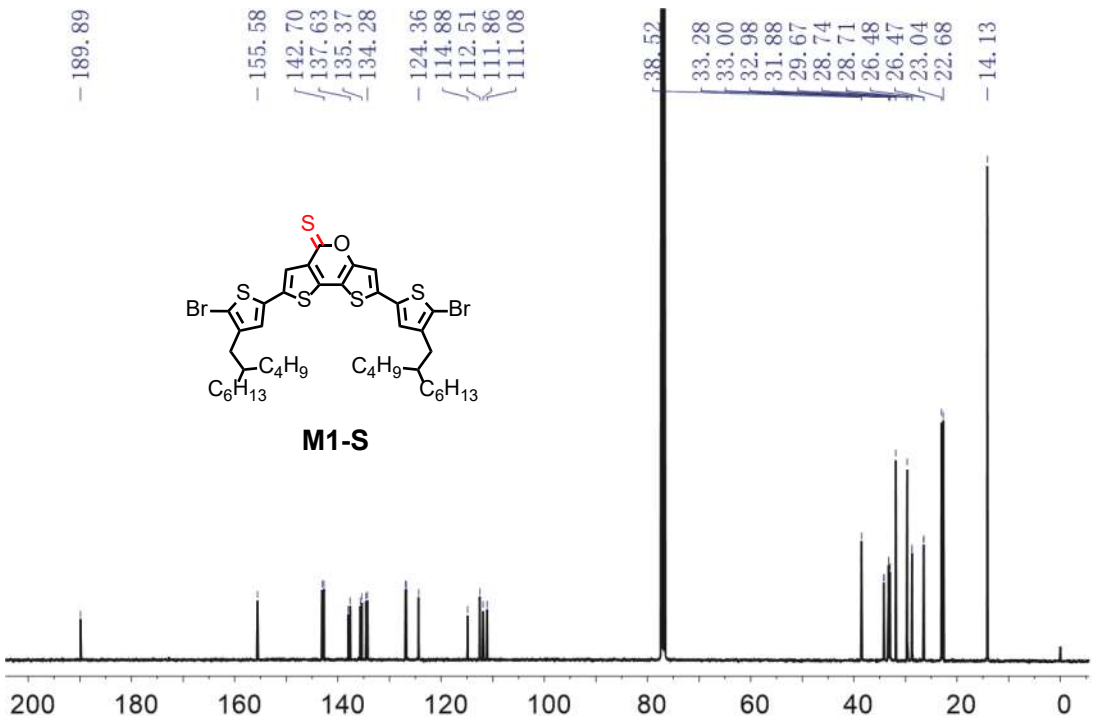

Fig. S4. ^{13}C NMR spectrum of M1-S.

4. FT-IR

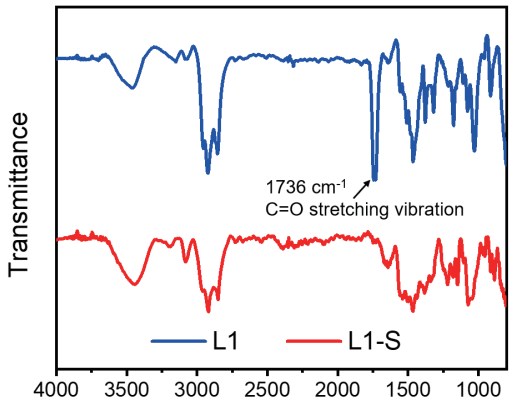

Fig. S5. FT-IR spectra for L1 and L1-S.

5. CV

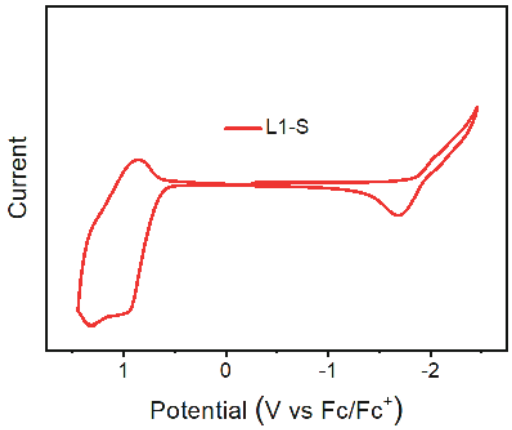

Fig. S6. Cyclic voltammogram for L1-S.

6. DFT

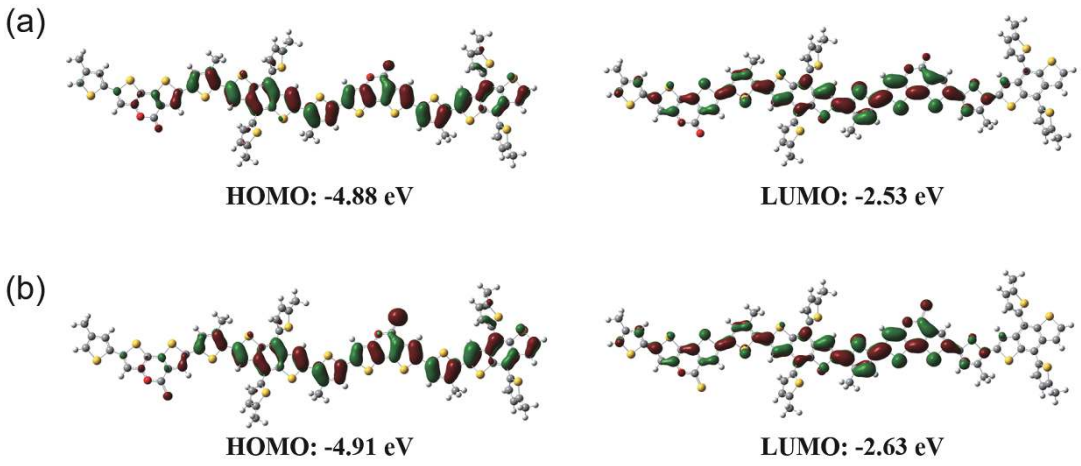

Fig. S7. DFT-predicted HOMO and LUMO for (a) L1 and (b) L1-S.

7. Device fabrication and measurements

Conventional solar cells

A 30 nm thick PEDOT:PSS layer was made by spin-coating an aqueous dispersion onto ITO glass (4000 rpm for 30 s). PEDOT:PSS substrates were dried at 150 °C for 10 min. A L1-S:BTP-eC9 (or L1:BTP-eC9) blend in chloroform (CF) was spin-coated onto PEDOT:PSS layer. PDIN (2 mg/mL) in MeOH: AcOH (1000 : 3) was spin-coated onto active layer (5000 rpm for 30 s). Ag (~80 nm) was evaporated onto PDIN through a shadow mask (pressure ca. 10^{-4} Pa). The effective area for the

devices is 4 mm^2. The thicknesses of the active layers were measured by using a KLA Tencor D-120 profilometer. *J–V* curves were measured by using a computerized Keithley 2400 SourceMeter and a Xenon-lamp-based solar simulator (Enli Tech, AM 1.5G, 100 mW/cm^2). The illumination intensity of solar simulator was determined by using a monocrystalline silicon solar cell (Enli SRC2020, 2 × 2 cm^2) calibrated by the National Institute of Metrology (NIM). The external quantum efficiency (EQE) spectra were measured by using a QE-R3011 measurement system (Enli Tech). The best cells were further tested at NIM for certification. A metal mask with an aperture (2.580 mm^2) was used to define the effective area.

Hole-only devices

The structure for hole-only devices is ITO/PEDOT:PSS/active layer/MoO_3/Al. A 30 nm thick PEDOT:PSS layer was made by spin-coating an aqueous dispersion onto ITO glass (4000 rpm for 30 s). PEDOT:PSS substrates were dried at 150 °C for 10 min. A pure L1-S (or L1) in CF or a L1-S:BTP-eC9 (or L1:BTP-eC9) blend in CF was spin-coated onto PEDOT:PSS layer. Finally, MoO_3 (~6 nm) and Al (~100 nm) was successively evaporated onto the active layer through a shadow mask (pressure ca. 10^{-4} Pa). *J–V* curves were measured by using a computerized Keithley 2400 SourceMeter in the dark.

Electron-only devices

The structure for electron-only devices is Al/active layer/Ca/Al. Al (~80 nm) was evaporated onto a glass substrate. A L1-S:BTP-eC9 (or L1:BTP-eC9) blend in CF was spin-coated onto Al. Ca (~5 nm) and Al (~100 nm) were successively evaporated onto the active layer through a shadow mask (pressure ca. 10^{-4} Pa). *J–V* curves were measured by using a computerized Keithley 2400 SourceMeter in the dark.

8. Optimization of device performance

Table S1. Optimization of D/A ratio for L1:BTP-eC9 solar cells[a].

D/A (w/w)	V_{oc} (V)	J_{sc} (mA/cm^2)	FF (%)	PCE (%)
1 : 0.8	0.828	25.12	75.9	15.79 (15.38)[b]
1 : 1	0.831	25.94	74.8	16.12 (16.05)
1 : 1.2	0.827	24.50	74.0	15.00 (14.71)
1 : 1.4	0.825	24.01	72.5	14.35 (14.21)

[a]Blend solution: 13 mg/mL in CF; spin-coating: 3500 rpm for 30 s.
[b]Data in parentheses stand for the average PCEs for 10 cells.

Table S2. Optimization of the active layer thickness for L1:BTP-eC9 solar cells[a].

Thickness (nm)	V_{oc} (V)	J_{sc} (mA/cm^2)	FF (%)	PCE (%)
120	0.829	25.92	73.4	15.77 (15.63)[b]
109	0.831	25.94	74.8	16.12 (16.05)
98	0.827	25.88	74.0	15.84 (15.75)
91	0.824	25.56	74.8	15.75 (15.50)
80	0.826	24.69	75.1	15.32 (15.29)

[a]D/A ratio: 1 : 1 (w/w); blend solution: 13 mg/mL in CF.
[b]Data in parentheses stand for the average PCEs for 10 cells.

Table S3. Optimization of CN content for L1:BTP-eC9 solar cells[a].

CN (vol%)	V_{oc} (V)	J_{sc} (mA/cm^2)	FF (%)	PCE (%)
0	0.831	25.94	74.8	16.12 (16.05)[b]
0.3	0.814	25.82	73.3	15.40 (15.31)
0.5	0.812	25.53	72.6	15.04 (14.99)
0.7	0.815	25.53	71.9	14.95 (14.69)

[a]D/A ratio: 1 : 1 (w/w); blend solution: 13 mg/mL in CF; spin-coating: 3500 rpm for 30 s.
[b]Data in parentheses stand for the average PCEs for 10 cells.

Table S4. Optimization of D/A ratio for L1-S:BTP-eC9 solar cells[a].

D/A (w/w)	V_{oc} (V)	J_{sc} (mA/cm^2)	FF (%)	PCE (%)
1 : 0.8	0.844	26.25	75.2	16.65 (16.59)[b]
1 : 1	0.844	26.79	76.3	17.23 (17.18)
1 : 1.2	0.843	26.05	75.2	16.50 (16.28)
1 : 1.4	0.843	26.05	72.2	15.85 (15.56)

[a]Blend solution: 13 mg/mL in CF; spin-coating: 4000 rpm for 30 s.
[b]Data in parentheses stand for the average PCEs for 10 cells.

Table S5. Optimization of the active layer thickness for L1-S:BTP-eC9 solar cells[a].

Thickness (nm)	V_{oc} (V)	J_{sc} (mA/cm^2)	FF (%)	PCE (%)
132	0.843	26.30	76.4	16.94 (16.90)[b]
122	0.844	26.79	76.3	17.23 (17.18)
110	0.845	27.22	77.1	17.73 (17.69)
101	0.845	26.00	77.9	17.10 (17.01)
88	0.843	25.65	77.4	16.74 (16.60)

[a]D/A ratio: 1 : 1 (w/w); blend solution: 13 mg/mL in CF.
[b]Data in parentheses stand for the average PCEs for 10 cells.

Table S6. Optimization of CN content for L1-S:BTP-eC9 solar cells[a].

CN (vol%)	V_{oc} (V)	J_{sc} (mA/cm^2)	FF (%)	PCE (%)
0	0.845	27.22	77.1	17.73(17.69)[b]
0.3	0.844	26.75	76.1	17.16 (16.97)
0.5	0.841	26.00	75.9	16.60 (16.43)
0.7	0.838	25.66	73.8	15.86 (15.79)

[a]D/A ratio: 1 : 1 (w/w); blend solution: 13 mg/mL in CF; spin-coating: 4000 rpm for 30 s.
[b]Data in parentheses stand for the average PCEs for 10 cells.

9. SCLC

Charge carrier mobility was measured by SCLC method. The mobility was determined by fitting the dark current to the model of a single carrier SCLC, which is described by:

$$J = \frac{9}{8}\varepsilon_0\varepsilon_r\mu\frac{V^2}{d^3},$$

where J is the current density, μ is the zero-field mobility of holes (μ_h) or electrons (μ_e), ε_0 is the permittivity of the vacuum, ε_r is the relative permittivity of the material, d is the thickness of the blend film, and V is the effective voltage ($V = V_{appl} - V_{bi}$, where V_{appl} is the applied voltage, and V_{bi} is the built-in potential determined by electrode work function difference). Here, $V_{bi} = 0.1$ V for hole-only devices, $V_{bi} = 0$ V for electron-only devices[2]. The mobility was calculated from the slope of $J^{1/2}$–V plot.

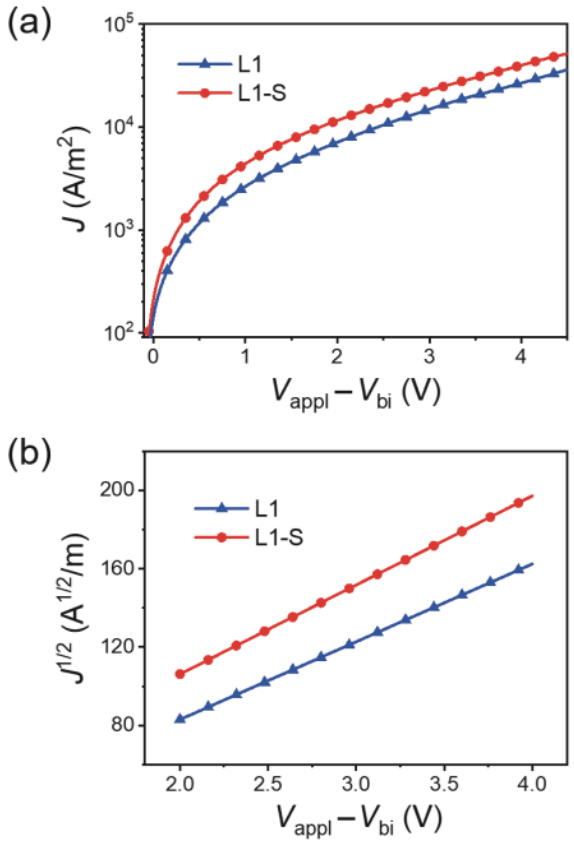

Fig. S8. J–V curves (a) and corresponding $J^{1/2}$–V plots (b) for the hole-only devices (in dark). The thicknesses for L1 and L1-S films are 104 and 119 nm, respectively.

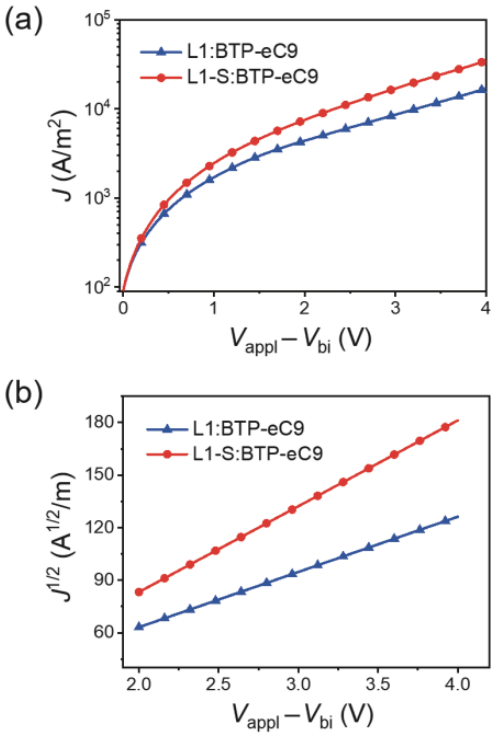

Fig. S9. *J*–*V* curves (a) and corresponding $J^{1/2}$–*V* plots (b) for the hole-only devices (in dark). The thicknesses for L1:BTP-eC9 (1 : 1) and L1-S:BTP-eC9 (1 : 1) blend films are 119 and 103 nm, respectively.

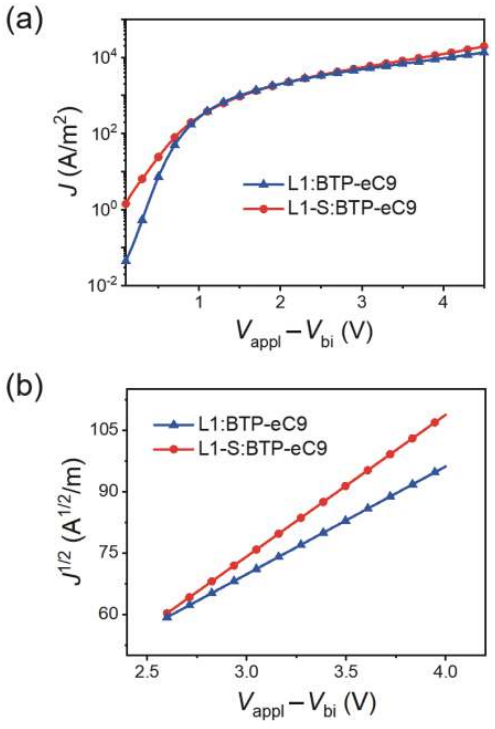

Fig. S10. *J*–*V* curves (a) and corresponding $J^{1/2}$–*V* plots (b) for the electron-only devices (in dark). The thicknesses for L1:BTP-eC9 (1 : 1) and L1-S:BTP-eC9 (1 : 1) blend films are 114 and 115 nm, respectively.

Table S7. Hole and electron mobilities.

Film	μ_h (cm^2/(V·s))	μ_e (cm^2/(V·s))	μ_h/μ_e
L1	5.93×10^{-4}	–	–
L1-S	1.17×10^{-3}	–	–
L1:BTP-eC9 (1 : 1)	5.60×10^{-4}	3.43×10^{-4}	1.63
L1-S:BTP-eC9 (1 : 1)	8.78×10^{-4}	6.09×10^{-4}	1.44

10. NIM certification for L1-S:BTP-eC9 solar cells

Appendix: Summary of the Report
Report No.: GXgf2020-50044
Client: The National Center for Nanoscience and Technology
Sample: Organic Solar Cells
Type/Model: Organic Solar Cells
DUT S/N: J24-M1-F-1
Manufacturer: The National Center for Nanoscience and Technology
Date of Test: 12/31/2020
Temperature Sensor/Control System: None
Environmental conditions: (22.9±1) C°, RH (29.0±2) %
Mask: An aperture area of 2.580 mm² (Certificate No.: CDjc2019-01321)

The test has been conducted by the PV Metrology Lab of NIM (National Institute of Metrology, China). Measurement of irradiance intensity and all other measurements are traceable to the International System of Units (SI). Data in this report apply only at the time of the test for the sample. For more details, please refer to the text of the report.

Forward Scan:

Area (mm^2)	I_{sc}(mA)	V_{oc}(V)	P_{max}(mW)
2.580	0.683	0.827	0.442
I_{max}(mA)	V_{max}(V)	FF (%)	η (%)
0.623	0.710	78.3	17.1

I-V Characterization Methods:
JJF 1622-2017: Calibration Specification of Solar Cells: Photoelectric Properties
Secondary Reference Cell:
Device S/N: 81#; Device Material: Mono-Si
Solar Simulator:
Classification: AAA (Double-light source: Xeon and Halogen);
Total irradiance: 1000 W/m² based on I_{sc} of the above Secondary Reference Cell.

Fig. S11. (Color online) NIM (Beijing) report for L1-S:BTP-eC9 solar cells.

11. Exciton dissociation probabilities

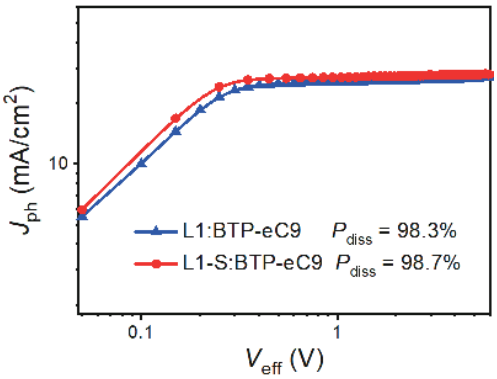

Fig. S12. J_{ph}–V_{eff} plots.

12. Bimolecular recombination

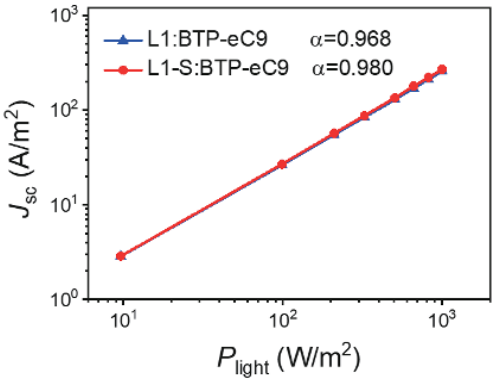

Fig. S13. J_{sc}–P_{light} plots.

13. AFM

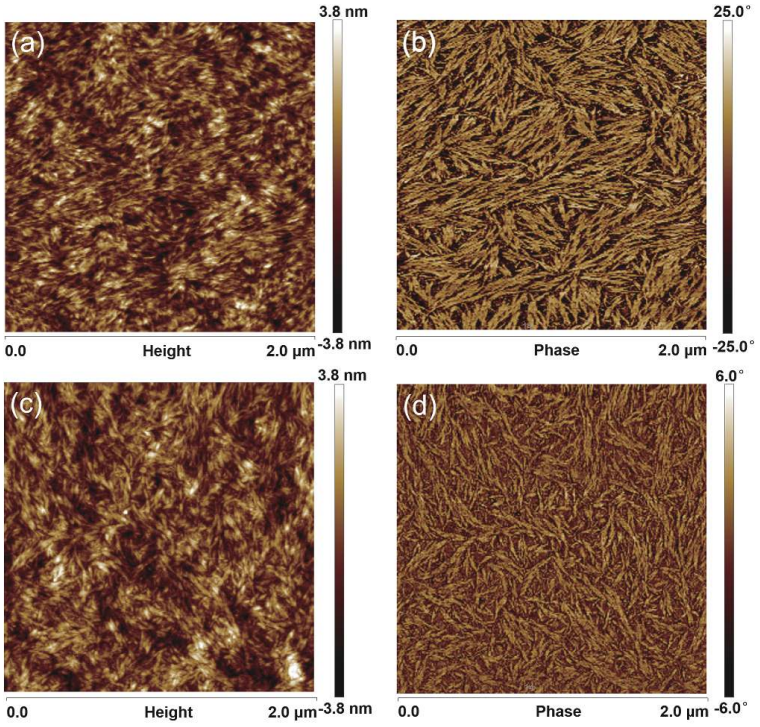

Fig. S14. (Color online) AFM height (left) and phase (right) images for the blend films. (a, b) L1:BTP-eC9 (R_{rms} = 9.94 nm); (c), d) L1-S:BTP-eC9 (R_{rms} = 2.07 nm). R_{rms}: root-mean-square roughness.

References

[1] Liu J, Liu L, Zuo C, et al. 5H-dithieno[3,2-b:2′,3′-d]pyran-5-one unit yields efficient wide-bandgap polymer donors. Sci Bull, 2019, 64, 1655

[2] Duan C, Cai W, Hsu B, et al. Toward green solvent processable photovoltaic materials for polymer solar cells: the role of highly polar pendant groups in charge carrier transport and photovoltaic behavior. Energy Environ Sci, 2013, 6, 3022